Implication of Parallel Velocity Gradient-Driven Instability with Hydrodynamic Electrons to SOL Width

Itsuki OYAMA and Yusuke KOSUGA[1)]

Interdisciplinary Graduate School of Engineering Science, Kyushu University, Kasuga, Fukuoka 816-8580, Japan
[1)]*Research Institute for Applied Mechanics, Kyushu University, Kasuga, Fukuoka 816-8580, Japan*

(Received 29 September 2023 / Accepted 29 February 2024)

Herein, a new aspect of the parallel velocity gradient (PVG)- driven instability is explored. We present its linear stability analysis and investigate the transport properties of the instability, focusing on a specific electron motion called hydrodynamic. In the realm of hydrodynamic electrons, electron motions across the magnetic field are much faster than those along the magnetic field. This electron motion plays an important role in fluctuation transport. This analysis reveals that the PVG convective cell is newly excited, and its feature of particle transport is favorable, since the particle pinch by PVG with adiabatic electrons disappears.

Keywords: PVG instability, transport, hydrodynamic electron, scrape-off layer

DOI: 10.1585/pfr.19.1403019

1. Introduction

Today, heat load toward divertors is one of the most crucial problems in fusion sciences. This heat load manifests in two types of phenomena. One is an abrupt heat load, well known as edge localized modes (ELMs) [1–3], and the other is the steady heat load. As the studies on ELM suppression progress [4], steady heat loads have gained attention these days in the context of the protection for the plasma-facing components via SOL broadening. Recently, the Eich scaling law satisfactorily described the SOL heat load width [5, 6], and Goldston [7] propounded a heuristic drift (HD) model for it, which perfectly fits the data of H-mode discharges. As is well known, this model is solely based on the drift motion by magnetic fields, the grad B and curv B drifts [7]. In this scaling, the power decay length is poorly estimated as small. For example, the length for ITER is approximately $1mm$, which prompted us to consider its handling. As previously mentioned, turbulence is not considered in the HD model. Therefore, turbulence should be a key SOL width handling element. Fluctuations are observed in SOL [8], which can drive fluxes from experimental perspective [9]. In this paper, we will demonstrate the behaviour of one of such fluctuations for SOL broadening.

Considering local fluctuations is important because they can play an important role in advanced operations, such as internal transport barriers with low confinement mode edge [10]. The contribution of turbulence to the SOL width is estimated using simple heuristic considerations [11]. Additionally, theoretical considerations are necessary to further explain its physical mechanism [12].

Parallel velocity along magnetic field lines in SOL can become subsonic in several devices [13, 14]. These flows lead to a radial gradient, which can drive instability, hereafter called as parallel velocity gradient (PVG) instability [15]. Lately, PVG has been studied theoretically [16–19], experimentally [20, 21] and using simulations [22, 23]. In [18,21], it is reported that PVG contributes to inward particle pinch, which can be disadvantageous for SOL broadening. However, PVG may change its transport feature in the future devices, such as in ITER. This is because ITER has longer major and minor radii, which affect the time scales of electron motions. Considering resistive drift wave as an example, excited fluctuations can be changed using electron motions based on the size of devices [24]. Particle transport changes its intensity, and especially, heat transport can change its direction. This alteration is governed by electron motions, which are electron drift frequency and electron parallel diffusion. Hence, we focused on PVG with altered electron motion.

We aim to reveal the altered transport features of PVG using specific electron motion based on the size of the devices. These features are described using a quasi-linear framework and are discussed in Sec. 2. The discussion and summary are presented in Sec. 3.

2. Model and Linear Analysis

With the aim to describe transport phenomena in the SOL region in fusion plasmas, we use the extended Hasegawa-Wakatani equation with parallel flow [17–19, 25]. As previously proposed, to demonstrate the fluctuation that we focus on, this model is represented as a simplified fluid description.

$$\frac{d}{dt}\rho_s^2\nabla_\perp^2\frac{e\phi}{T_e} = -D_\parallel\nabla_\parallel^2\left(\frac{e\phi}{T_e}-\frac{n_e}{n_0}\right),$$

author's e-mail: oyama.itsuki.582@s.kyushu-u.ac.jp

$$\frac{d}{dt}\frac{n_e}{n_0} + \nabla_\parallel v_\parallel = -D_\parallel \nabla_\parallel^2 \left(\frac{e\phi}{T_e} - \frac{n_e}{n_0}\right),$$
$$\frac{d}{dt} v_\parallel = -c_s^2 \nabla_\parallel \frac{n_e}{n_0},$$

where $d/dt = \partial_t + (c/B)\hat{z}\times\nabla\phi\cdot\nabla$ is the total derivative including the nonlinear $E\times B$ convection, c_s is the ion sound velocity, ρ_s is the ion sound larmor radius, $D_\parallel = v_{the}^2/\nu_{ei}$ is the parallel electron diffusion, ϕ is the electrostatic potential, n is density, and $v_\parallel$ is the parallel flow. The system is defined as a cylindrical system. The correspondence $\parallel \leftrightarrow z$ and $\perp \leftrightarrow (r,\theta) \leftrightarrow (x,y)$ in the cylindrical coordinate system is understood hereafter.

To elucidate the instability caused by parallel flow shear, we obtain a set of equations by linearization and Fourier analysis, as shown below:

$$i\omega\rho_s^2 k_\perp^2 \hat{\phi}_{\boldsymbol{k}} = -D_\parallel k_\parallel^2 (\hat{n}_{\boldsymbol{k}} - \hat{\phi}_{\boldsymbol{k}}), \tag{1}$$
$$-i\omega\hat{n}_{\boldsymbol{k}} + i\omega_{*e}\hat{\phi}_{\boldsymbol{k}} + ik_\parallel \tilde{v}_{i,\boldsymbol{k}} = -D_\parallel k_\parallel^2 (\hat{n}_{\boldsymbol{k}} - \hat{\phi}_{\boldsymbol{k}}), \tag{2}$$
$$-i\omega\tilde{v}_{i,\boldsymbol{k}} - \frac{c}{B} ik_y \tilde{\phi}_{\boldsymbol{k}} \langle v_z\rangle' = -\frac{e}{m_i} ik_z \tilde{\phi}_{\boldsymbol{k}}. \tag{3}$$

Here, it is useful to denote normalized quantities by $\tilde{n}_e/n_0 \to \hat{n}$ and $e\tilde{\phi}/T_e \to \hat{\phi}$. $\langle\ldots\rangle$ denotes the averaged quantities over θ and $\parallel$ direction. $\omega_{*e} = k_y\rho_s(c_s/L_n)$ is the electron drift frequency and $L_n^{-1} = -\langle n\rangle'/n_0$ is the scale length of the density. Here $\ldots'$ represents the radial differential. We assume that the wavelength of the fluctuation is shorter than the typical scale length of equilibrium quantities. Subsequently, the density and parallel velocity responses are obtained as follows:

$$\hat{n}_{\boldsymbol{k}} = \left(\frac{\omega_{*e}}{\omega} - \rho_s^2 k_\perp^2\right)\hat{\phi}_{\boldsymbol{k}} + \frac{k_\parallel}{\omega}\tilde{v}_{\parallel,\boldsymbol{k}}, \tag{4}$$
$$\tilde{v}_{i,\boldsymbol{k}} = c_s\left(\frac{c_s k_\parallel}{\omega} - \frac{k_y\rho_s\langle v_z\rangle'}{\omega}\right)\hat{\phi}_{\boldsymbol{k}}. \tag{5}$$

Substituting Eq.(4) and Eq.(5) into Eq.(1), we obtain the following general dispersion relation:

$$-i\frac{\rho_s^2 k_\perp^2}{D_\parallel k_\parallel^2}\omega = -(1+\rho_s^2 k_\perp^2) + \frac{\omega_{*e}}{\omega} + \frac{k_\parallel^2 c_s^2}{\omega^2}\left(1 - \frac{\rho_s k_y \langle v_z\rangle'}{k_\parallel c_s}\right). \tag{6}$$

This dispersion relation Eq.(6) has a general form, which includes several fluctuations, drift wave (lower left), drift convective cell (lower right), and PVG (upper left), as shown in Fig. 1. Because Eq.(6) is a cubic equation for ω, we can use a well-known algebraic method to solve this cubic equation, which is called the Cardano's fomula [26]. Solving Eq.(6) using the Cardano's formula, we will systematically obtain the following:

$$\omega = u - \frac{p}{3u} - \frac{A}{3}, \tag{7}$$

where

$$u = \left\{-\frac{q}{2} \pm \frac{1}{2}\sqrt{q^2 + \frac{4}{27}p^3}\right\}^{1/3},$$

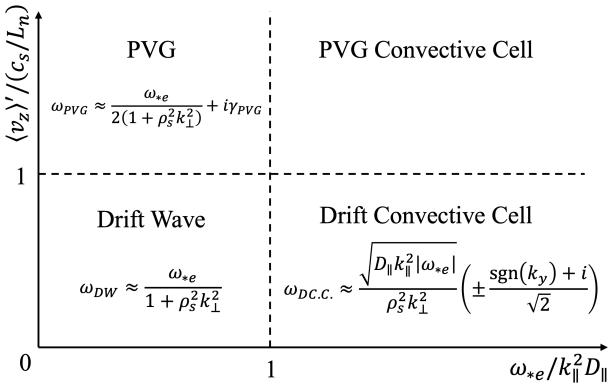

Fig. 1 Schematic graph : region corresponding to each fluctuation. Vertical axis corresponds to the ratio of $\langle v_z\rangle'$ to c_s/L_n and parallel axis corresponds to the ratio of ω_{*e} to $k_\parallel^2 D_\parallel$.

$$p = -i\frac{k_\parallel^2 D_\parallel}{\rho_s^2 k_\perp^2}\omega_{*e} + \frac{k_\parallel^4 D_\parallel^2}{3\rho_s^4 k_\perp^4}(1+\rho_s^2 k_\perp^2)^2,$$
$$A = i\frac{k_\parallel^2 D_\parallel}{\rho_s^2 k_\perp^2}(1+\rho_s^2 k_\perp^2),$$

and

$$q = -2i\frac{k_\parallel^6 D_\parallel^3}{27\rho_s^6 k_\perp^6}(1+\rho_s^2 k_\perp^2)^3 - \frac{k_\parallel^4 D_\parallel^2 \omega_{*e}}{3\rho_s^4 k_\perp^4}(1+\rho_s^2 k_\perp^2) - i\frac{k_\parallel^2 D_\parallel k_\parallel^2 c_s^2}{\rho_s^2 k_\perp^2}\left(1 - \frac{k_y\rho_s}{k_\parallel c_s}\langle v_z\rangle'\right).$$

Equation (7) obviously contains other fluctuations shown in Fig. 1. Taking drift wave as an example, we can derive the dispersion relation of drift wave from Eq.(7) using $\omega_{*e}/D_\parallel k_\parallel^2 \ll 1$ as the expansion parameter and neglecting the flow shear. Then, we obtain:

$$\begin{aligned}
\omega_{DW} &= u - \frac{p}{3u} - \frac{A}{3} \\
&\approx \frac{i^{1/3}}{3}\frac{k_\parallel^2 D_\parallel}{\rho_s^2 k_\perp^2}(1+\rho_s^2 k_\perp^2) \\
&\quad\times\left[1 + \frac{\pm\sqrt{3} - 3i}{2}\frac{\rho_s^2 k_\perp^2}{k_\parallel^2 D_\parallel}\frac{\omega_{*e}}{(1+\rho_s^2 k_\perp^2)^2}\right] \\
&\quad - \frac{1}{3i^{1/3}}\frac{k_\parallel^2 D_\parallel}{\rho_s^2 k_\perp^2}(1+\rho_s^2 k_\perp^2) \\
&\quad\times\left[1 - \frac{\pm\sqrt{3} + 3i}{2}\frac{\rho_s^2 k_\perp^2}{k_\parallel^2 D_\parallel}\frac{\omega_{*e}}{(1+\rho_s^2 k_\perp^2)^2}\right] \\
&\quad - \frac{i}{3}\frac{k_\parallel^2 D_\parallel}{\rho_s^2 k_\perp^2}(1+\rho_s^2 k_\perp^2) \\
&= \frac{\omega_{*e}}{1+\rho_s^2 k_\perp^2},
\end{aligned}$$

where $O(\omega_{*e}/D_\parallel k_\parallel^2) \ll 1$ is assumed. With flow shear, the dispersion relation of PVG (upper left in Fig. 1) can be clearly obtained from Eq.(7).

2.1 PVG convective cell

In this section, we discuss the fluctuation with the hydrodynamic electron response, i.e., $\omega_{*e}/D_{\parallel}k_{\parallel}^2 \gg 1$. In this case, the electron motion resembles that of a quasi-two-dimensional vortex perpendicular to the toroidal plane. The expansion parameter in this case is $D_{\parallel}k_{\parallel}^2/\omega_{*e} \ll 1$. When this expansion parameter becomes valid, this limitation corresponds to a small $k_{\parallel}$. The assumption regarding the wave number parallel to the magnetic field line is regarded as $k_{\parallel} = 1/qR$. qR is the product of the safety factor q and major radius R. Taking the safety factor as $q_{95} \sim 3$, with some simplifications, the electron response shall be proportional to the size of devices. In [24], this hydrodynamic electron regime can be easily found in large devices, e.g., ITER. Accordingly, these limitations relevant to the parallel flow shear and electron motion laid the foundation for the desired discussion.

Further, we show the dispersion relation for the PVG convective cell. The PVG convective cell is the new regime of this system. In addition, we demonstrate modes in the PVG convective cell. Using the hydrodynamic electron regime $k_{\parallel}^2 D_{\parallel}/\omega_{*e} \ll 1$ as the expansion parameter in Eq.(7), we obtain:

$$\omega \approx \left(-i \frac{k_{\parallel}^2 D_{\parallel} k_{\parallel} c_s k_y \rho_s \langle v_z \rangle'}{\rho_s^2 k_{\perp}^2} \right)^{1/3}. \tag{8}$$

Furthermore, we can directly derive Eq.(8) from Eq.(6) using the same assumption as above. In a direct comparison between the first term in the LHS and last term in the RHS of Eq.(6), we can obtain the same dispersion relation as Eq.(8).

$$-i \frac{\rho_s^2 k_{\perp}^2}{D_{\parallel} k_{\parallel}^2} \omega \sim -\frac{k_{\parallel} c_s \rho_s k_y \langle v_z \rangle'}{\omega^2}.$$

Moreover, we can derive this dispersion relation from Eq.(1), Eq.(2) and Eq.(3). Assuming $\langle v_z \rangle'$ is sufficiently large, the velocity fluctuation is activated only by the parallel flow shear in Eq.(5).

$$\tilde{v}_{i,\boldsymbol{k}} \sim -\frac{c_s k_y \rho_s \langle v_z \rangle'}{\omega} \hat{\phi}_{\boldsymbol{k}}. \tag{9}$$

Substituting this into Eq.(2), the density fluctuation is found to be strongly activated by the parallel flow shear.

$$\hat{n}_{\boldsymbol{k}} \sim -\frac{k_{\parallel} c_s k_y \rho_s}{\omega^2} \langle v_z \rangle' \hat{\phi}_{\boldsymbol{k}}. \tag{10}$$

Further, we determine the behavior of the PVG convective cells from the vorticity equation, Eq.(1). Its expression corresponds to Eq.(8). Thus, vorticity is strongly affected by the parallel flow shear.

We now focus on the value of $(\pm i)^{1/3}$. Here, the sign is determined by the sign of $k_{\parallel}k_y\langle v_z \rangle'$. We take positive sign for $k_{\parallel}k_y\langle v_z \rangle' < 0$ and vice versa. Note that the Euler's formula, Eq.(8), takes the following forms due to the contraction of the trigonometric function.

$$\omega = \left(\pm \frac{\sqrt{3}}{2} + \frac{i}{2} \right) \sigma, \tag{11}$$

and

$$\omega = i\sigma, \tag{12}$$

where

$$\sigma = \left| \frac{k_{\parallel}^2 D_{\parallel} k_{\parallel} c_s k_y \rho_s \langle v_z \rangle'}{\rho_s^2 k_{\perp}^2} \right|^{1/3}. \tag{13}$$

Briefly, we refer to Eq.(11) as the oscillatory mode and Eq.(12) as the pure growth mode. These are named after the physical pictures of these waves in a real space. In the oscillatory mode, the amplitudes of waves increase with oscillation in the real space and propagate as time passes; this represents the travailing mode. Furthermore, the direction of v_z and its gradient have a certain meaning for its propagation direction. This is because the direction of $\langle v_z \rangle'$ imposes constraints over $k_{\parallel}$ and k_y. For example, when the sign of $\langle v_z \rangle'$ is positive, the sign of the product $k_{\parallel}k_y$ must be negative to meet the condition to be excited. Considering the phase velocities $\omega/k_{\parallel}$ and ω/k_y, it can be easily seen that the sign of $\langle v_z \rangle'$ determines the propagation direction of this traveling mode. In the pure growth mode, the amplitudes of waves increase exponentially without propagating in the real space.

The excitation of these modes depends on the sign of σ in Eq.(13), and the component $k_{\parallel}k_y\langle v_z \rangle'$ is responsible for its sign. Considering the imaginary parts of Eq.(11) and Eq.(12), for exciting the oscillatory mode, the sign of $k_{\parallel}k_y\langle v_z \rangle'$ must be negative. Meanwhile, when the sign of $k_{\parallel}k_y\langle v_z \rangle'$ is positive, the pure growth mode can be excited. In summary, if $k_{\parallel}k_y\langle v_z \rangle' \neq 0$, either the oscillatory or pure growth mode can be chosen. Compared with other regimes, especially PVG [19], we can evaluate this as a broader condition. This is because a PVG with adiabatic electrons demands $k_{\parallel}k_y\langle v_z \rangle' > 0$.

In addition, $k_{\parallel}k_y\langle v_z \rangle'$ is the component that determines the time evolution of vorticity. Especially, $k_{\parallel}k_y\langle v_z \rangle'$ is excited from the compression term in Eq.(2). The excitation of these distinctive modes is regulated by the compressibility, which has also been discussed previously, e.g., in [17, 27].

2.2 Fluctuation

In each mode, the density and momentum fluctuations are derived from Eq.(9) and Eq.(10), respectively. In the oscillatory mode, we obtain density fluctuation as:

$$\tilde{n}_{osc,\boldsymbol{k}} = -\frac{k_{\parallel} c_s k_y \rho_s \langle v_z \rangle'}{2\sigma^2} (1 \mp i\sqrt{3}) \tilde{\phi}_{\boldsymbol{k}}. \tag{14}$$

In the above equation, phase differences exist between the density and electrostatic potential fluctuations. Thus, we

can expect finite particle transport in this mode. Furthermore, we can obtain the momentum fluctuation in the oscillatory mode as:

$$\tilde{v}_{\parallel,osc,\boldsymbol{k}} = -\frac{k_y c_s \rho_s \langle v_z \rangle'}{2\sigma}(i \mp \sqrt{3})\tilde{\phi}_{\boldsymbol{k}}.$$

Additionally, finite phase differences exist between the velocity and electrostatic potential fluctuations. Therefore, we can expect finite momentum transport in this mode.

In the pure growth mode, we obtain the density fluctuation as:

$$\tilde{n}_{pg,\boldsymbol{k}} = \frac{k_\parallel c_s k_y \rho_s \langle v_z \rangle'}{\sigma^2}\tilde{\phi}_{\boldsymbol{k}}. \tag{15}$$

Considering this, we cannot expect net particle transport in this mode because no phase difference exists between the density and electrostatic potential fluctuations. In addition, we can obtain momentum fluctuation in the pure growth mode as

$$\tilde{v}_{\parallel,pg,\boldsymbol{k}} = -i\frac{c_s k_y \rho_s \langle v_z \rangle'}{\sigma}\tilde{\phi}_{\boldsymbol{k}}.$$

Hence, we can, likewise as to the oscillatory mode, expect finite momentum transport in the pure growth mode.

2.3 Transport

In this section, we focus on the transport features of PVG convective cells using quasi-linear analysis [28]. We will perform each calculation for the oscillatory and pure growth modes. In the quasi-linear analysis, the particle flux caused by fluctuating $E \times B$ drift is given by $\Gamma = \langle \tilde{V}_{E\times B}\tilde{n} \rangle$. Analogously, the momentum flux is given by $\Pi_{rz} = \langle \tilde{V}_{E\times B}\tilde{v}_\parallel \rangle$.

In the oscillatory mode, each flux can be calculated as follows. Starting from the density flux in the oscillatory mode, we can get

$$\begin{aligned}
\Gamma_{osc} &= \langle \tilde{V}_{E\times B}\tilde{n}_{osc} \rangle \\
&= \left\langle -\frac{ik_y}{B_0}\tilde{\phi}_{\boldsymbol{k}} \cdot -\frac{k_\parallel c_s k_y \rho_s \langle v_z \rangle'}{2\sigma^2}(1 \mp i\sqrt{3})\tilde{\phi}_{\boldsymbol{k}} \right\rangle, \\
Re[\Gamma_{osc}] &= \left\langle \pm\sqrt{3}\frac{k_\parallel c_s k_y \rho_s \cdot k_y}{2\sigma^2 \cdot B_0}|\tilde{\phi}_{\boldsymbol{k}}|^2 \langle v_z \rangle' \right\rangle \\
&= \Gamma^+_{osc} + \Gamma^-_{osc} \\
&\approx 0.
\end{aligned}$$

Because the real parts of Γ_{osc} can only contribute to particle transport, there are equal volumes of transport in the opposite direction, as shown above. Contrary to our expectation from Eq.(14), there was no particle transport here because they cancel each other. Momentum flux in this mode is calculated as follows:

$$\begin{aligned}
\Pi_{rz,osc} &= \langle \tilde{V}_{E\times B}\tilde{v}_{\parallel,osc} \rangle \\
&= \left\langle -\frac{ik_y}{B_0}\tilde{\phi}_{\boldsymbol{k}} \cdot -\frac{c_s k_y \rho_s \langle v_z \rangle'}{2\sigma}(i \mp \sqrt{3})\tilde{\phi}_{\boldsymbol{k}} \right\rangle \\
&= \left\langle \frac{c_s k_y \rho_s \cdot k_y}{2\sigma \cdot B_0}(-1 \mp i\sqrt{3})|\tilde{\phi}_{\boldsymbol{k}}|^2 \right\rangle, \\
Re[\Pi_{rz,osc}] &= -\sum_k \frac{c_s^2 k_y^2 \rho_s^2}{2\sigma}|\hat{\phi}_{\boldsymbol{k}}|^2 \langle v_z \rangle' \\
&= -D_{v,osc}\langle v_z \rangle'.
\end{aligned} \tag{16}$$

Here $D_{v,osc} = \sum_k (c_s^2 k_y^2 \rho_s^2/2\sigma)|\hat{\phi}_{\boldsymbol{k}}|^2$. Because the real parts of $\Pi_{rz,osc}$ can, likewise as to particle flux, contribute to momentum transport, there is finite momentum transport. From Eq.(16), this momentum transport can be formed as the eddy viscosity on flow. This eddy viscosity characterizes momentum flux. When exciting the oscillatory mode, its momentum flux is down the gradient.

In the pure growth mode, we can also calculate each flux as follows. Beginning from the density flux in the pure growth mode, we obtain

$$\begin{aligned}
\Gamma_{pg} &= \langle \tilde{V}_{E\times B}\tilde{n}_{pg} \rangle \\
&= \left\langle -\frac{ik_y}{B_0}\tilde{\phi}_{\boldsymbol{k}} \cdot \frac{k_\parallel c_s k_y \rho_s \langle v_z \rangle'}{\sigma^2}\tilde{\phi}_{\boldsymbol{k}} \right\rangle, \\
Re[\Gamma_{pg}] &= 0.
\end{aligned}$$

As expected from Eq.(15), no finite particle transport is observed in this mode. This is obvious because the density fluctuations are in phase with the electrostatic potential fluctuations in Eq.(15). The momentum flux in this mode is calculated as follows:

$$\begin{aligned}
\Pi_{rz,pg} &= \langle \tilde{V}_{E\times B}\tilde{v}_{\parallel,pg} \rangle \\
&= \left\langle -\frac{ik_y}{B_0}\tilde{\phi}_{\boldsymbol{k}} \cdot -i\frac{c_s k_y \rho_s \langle v_z \rangle'}{\sigma}\tilde{\phi}_{\boldsymbol{k}} \right\rangle, \\
Re[\Pi_{rz,pg}] &= -\sum_k \frac{c_s^2 \rho_s^2 k_y^2}{\sigma}|\hat{\phi}_{\boldsymbol{k}}|^2 \langle v_z \rangle' \\
&= -D_{v,pg}\langle v_z \rangle'.
\end{aligned} \tag{17}$$

Here $D_{v,pg} = \sum_k (c_s^2 \rho_s^2 k_y^2/\sigma)|\hat{\phi}_k|^2$. This momentum flux has a real part, which contributes to momentum transport. As with the case of the pure growth mode, this flux can be formed as the eddy viscosity in Eq.(17). When the pure growth mode is excited, its momentum flux is down the gradient.

3. Summary and Discussion

Herein, the linear stability analysis and transport features of the PVG convective cell are explored theoretically. The PVG convective cell can be excited when the time scale of the electron motion across the magnetic field becomes shorter than that of electron diffusion along the magnetic field, in addition to a strong parallel flow shear. This electron response is characterized by the so-called hydrodynamic response, while it gets an adiabatic response in an opposite relation for these time scales. Comparing PVG with adiabatic electrons, the PVG convective cell has a broad condition for $k_y k_\parallel \langle v_z \rangle'$ for instability. A PVG convective cell can be destabilized with $k_y k_\parallel \langle v_z \rangle' \neq 0$, while

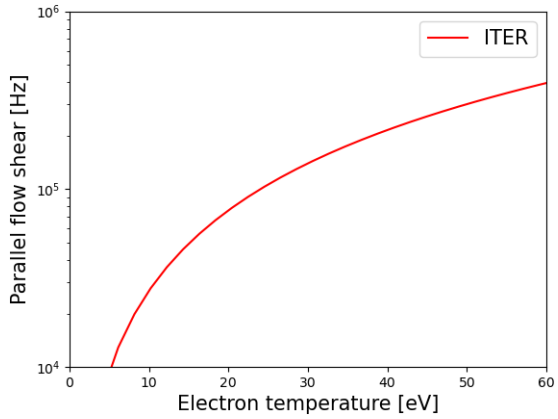

Fig. 2 This is the plot of Eq.(18). Parallel axis corresponds to the electron temperature [eV] and vertical axis corresponds to the parallel flow shear [Hz].

PVG with adiabatic electrons can only be destabilized with $k_y k_\parallel \langle v_z \rangle' > 0$. Two distinctive modes are found when the PVG convective cell is excited: the oscillatory and pure growth modes. The oscillatory mode is characterized by spatial propagation, while the pure growth mode is not. Moreover, density fluctuations exhibit phase differences in the oscillatory mode, which is unlikely to occur in the pure growth mode, while parallel velocity fluctuations in both modes demonstrate phase differences.

For transport, these two modes share their transport characteristics. Momentum flux is characterized by eddy viscosity, which relaxes the parallel velocity gradient when either of the modes is excited. Meanwhile, particle flux does not contribute to transport in either modes. Note that the mechanisms that lead to these particle transports are different from each other. In the oscillatory mode, because the same amount of finite particle transport can be conveyed in the opposite direction, these fluxes cancel each other. In contrast, in the pure growth mode, because its density and electrostatic potential fluctuations are in phase with each other, its particle flux is not originally generated. Owing to these results, the PVG convective cell cannot sufficiently broaden the SOL width to protect divertor plates from heat loads. However, compared with PVG with adiabatic electrons, a PVG convective cell can help passively to achieve this purpose. This is because the pinch effect caused by PVG with adiabatic electrons disappears in the PVG convective cell.

In the discussion, we mention the excitation of PVG convective cells. As previously mentioned in Sec. 2.1, the time scale for parallel velocity ($\nabla_\parallel v_i$) is dominant over the time scale for drift motion (ω_{*e}) in the PVG convective cell. Additionally, we can identify the region where the PVG convective cell is likely to be excited using $v_{*e}\partial_y\hat{\phi} \leq \nabla_\parallel \tilde{v}_i$. This leads to the comparison between the second and third terms on the LHS of (2). Concerning $\nabla_\parallel \tilde{v}_i$, it is obvious to obtain $\nabla_\parallel \tilde{v}_i$ from Eq.(9). Then the comparison of the magnitude between $v_{*e}\partial_y\hat{\phi}$ and $\nabla_\parallel \tilde{v}_i$ is obtained as

$$\frac{k_\parallel c_s k_y \rho_s \langle v_z \rangle'}{\omega} \geq k_y \rho_s \frac{c_s}{L_n},$$
$$\langle v_z \rangle' \geq \frac{c_s}{L_n} \sqrt{\frac{c_s}{L_n} \frac{m_i/m_e}{\nu_{e,i}}}. \tag{18}$$

Here we assume $\rho_s k_\perp \sim 1$ and $k_y/k_\perp \sim 1$. L_n is taken as minor radii, thus L_n is 2[m] in ITER. Taking m_i/m_e as the usual physical constant, it is approximately 1.8×10^3. $\nu_{e,i}$ is the electron collision frequency. Considering the case of a large device like ITER, we can assume c_s/L_n as approximately equal to 100 [kHz]. Plotting Eq.(18) in the range of 0 to 60 [eV], the curve is proportional to $T_e^{3/2}$ in ν_{ei}. Finally, we obtain Fig. 2. The PVG convective cell can be excited for values above the curve in Fig. 2.

Acknowledgments

We are grateful to the useful discussions with participants of APTWG 2023. This work was partly supported by the Grants-in-Aid for Scientific Research of JSPS of Japan (JP21H01066), a joint research project at RIAM, Kyushu University.

[1] H. Zohm, Edge localized modes (elms), Plasma Phys. Control. Fusion **38**(2),105 (1996).
[2] P.B. Snyder, H.R. Wilson, J.R. Ferron, L.L. Lao, A.W. Leonard, T.H. Osborne, A.D. Turnbull, D. Mossessian, M. Murakami and X.Q. Xu, Edge localized modes and the pedestal: A model based on coupled peeling–ballooning modes, Phys. Plasmas **9**(5), 2037 (2002).
[3] A.W. Leonard, Edge-localized-modes in tokamaks, Phys. Plasmas **21**(9) (2014).
[4] E. Viezzer, M.E. Austin, M. Bernert, K.H. Burrell, P. Cano-Megias, X. Chen, D.J. Cruz-Zabala, S. Coda, M. Faitsch, O. Février, L. Gil, C. Giroud, T. Happel, G.F. Harrer, A.E. Hubbard, J.W. Hughes, A. Kallenbach, B. Labit, A. Merle, H. Meyer, C. Paz-Soldan, P. Oyola, O. Sauter, M. Siccinio, D. Silvagni and E.R. Solano, Prospects of core–edge integrated no-elm and small-elm scenarios for future fusion devices, Nucl. Mater. Energy **34,** 101308 (2023).
[5] T. Eich, B. Sieglin, A. Scarabosio, W. Fundamenski, R.J. Goldston and A. Herrmann, Inter-elmpower decay length for jet and asdex upgrade: Measurement and comparison with heuristic drift-based model, Phys. Rev. Lett. **107**, 215001 (Nov. 2011).
[6] T. Eich, A.W. Leonard, R.A. Pitts, W. Fundamenski, R.J. Goldston, T.K. Gray, A. Herrmann, A. Kirk, A. Kallenbach, O. Kardaun, A.S. Kukushkin, B. LaBombard, R. Maingi, M.A. Makowski, A. Scarabosio, B. Sieglin, J. Terry, A. Thornton, ASDEX Upgrade Team, and JET EFDA Contributors, Scaling of the tokamak near the scrape-off layer h-mode power width and implications for iter, Nucl. Fusion **53**(9), 093031 (Aug. 2013).
[7] R.J. Goldston, Heuristic drift-based model of the power scrape-off width in low-gas-puff h-mode tokamaks, Nucl. Fusion **52**(1), 013009 (Dec. 2011).
[8] S.J. Zweben, J.A. Boedo, O. Grulke, C. Hidalgo, B. LaBombard, R.J. Maqueda, P. Scarin, and J.L. Terry, Edge turbulence measurements in toroidal fusion devices, Plasma Phys. Control. Fusion **49**(7), S1 (2007).

[9] A.J. Wootton, M.E. Austin, R.D. Bengtson, J.A. Boedo, R.V. Bravenec, D.L. Brower, J.Y. Chen, G. Cima, P.H. Diamond, R.D. Durst *et al*., Fluctuations and anomalous transport (in tokamaks, particularly text), Plasma Phys. Control. Fusion **30**(11), 1479 (1988).

[10] C.M. Greenfield, J.C. DeBoo, T.C. Luce, B.W. Stallard, E.J. Synakowski, L.R. Baylor, K.H. Burrell, T.A. Casper, E.J. Doyle, D.R. Ernst *et al*., Understanding and control of transport in advanced tokamak regimes in diii-d, Phys. Plasmas **7**(5), 1959 (2000).

[11] J.R. Myra, D.A. D'Ippolito and D.A. Russell, Turbulent transport regimes and the scrape-off layer heat flux width, Phys. Plasmas **22**(4), 042516 (2015).

[12] M. Giacomin, A. Stagni, P. Ricci, J.A. Boedo, J. Horacek, H. Reimerdes and C.K. Tsui, Theory-based scaling laws of near and far scrape-off layer widths in single-null l-mode discharges, Nucl. Fusion **61**(7), 076002 (2021).

[13] N. Asakura, ITPA SOL, and Divertor Topical Group, Understanding the sol flow in l-mode plasma on divertor tokamaks, and its influence on the plasma transport, J. Nucl. Mater. **363**, 41 (2007).

[14] J.A. Boedo, Edge turbulence and sol transport in tokamaks, J. Nucl. Mater. **390**, 29 (2009).

[15] N. D'Angelo, Kelvin—helmholtz instability in a fully ionized plasma in a magnetic field, Phys. Fluids **8**(9), 1748 (1965).

[16] X. Garbet, C. Fenzi, H. Capes, P. Devynck and G. Antar, Kelvin–helmholtz instabilities in tokamak edge plasmas, Phys. Plasmas **6**(10), 3955 (1999).

[17] Y. Kosuga, S.-I. Itoh and K. Itoh, Density peaking by parallel flow shear driven instability, Plasma Fusion Res. **10**, 3401024 (2015).

[18] Y. Kosuga, S.-I. Itoh and K. Itoh, Turbulence dynamics with the coupling of density gradient and parallel velocity gradient in the edge plasmas, Contrib. Plasma Phys. **56**(6-8), 511 (2016).

[19] Y. Kosuga, S.-I. Itoh and K. Itoh, Zonal flow generation in parallel flow shear driven turbulence, Phys. Plasmas **24**(3), 032304 (2017).

[20] T. Kaneko, H. Tsunoyama and R. Hatakeyama, Drift-wave instability excited by field-aligned ion flow velocity shear in the absence of electron current, Phys. Rev. Lett. **90**(12), 125001 (2003).

[21] S. Inagaki, T. Kobayashi, Y. Kosuga, S.-I. Itoh, T. Mitsuzono, Y. Nagashima, H. Arakawa, T. Yamada, Y. Miwa, N. Kasuya *et al*., A concept of cross-ferroic plasma turbulence, Scientific Reports **6**(1), 22189 (2016).

[22] D.R. McCarthy, A.E. Booth, J.F. Drake and P.N. Guzdar, Three-dimensional simulations of the parallel velocity shear instability, Phys. Plasmas **4**(2), 300 (1997).

[23] O.E. Garcia, V. Naulin, A.H. Nielsen and J.J. Rasmussen, Computations of intermittent transport in scrape-off layer plasmas, Phys. Rev. Lett. **92**, 165003 (Apr. 2004).

[24] S. Arai and Y. Kosuga, Characteristics of density and temperature fluctuation in fusion edge plasma and implication on scrape off layer width, Plasma Fusion Res. **17**, 1403050 (2022).

[25] A. Hasegawa and M. Wakatani, Plasma edge turbulence, Phys. Rev. Lett. **50**(9), 682 (1983).

[26] R. Wituła and D. Słota, Cardano's formula, square roots, chebyshev polynomials and radicals, J. Math. Anal. Appl. **363**(2), 639 (2010).

[27] J.C. Li and P.H. Diamond, Negative viscosity from negative compressibility and axial flow shear stiffness in a straight magnetic field, Phys. Plasmas **24**(3), 032117 (2017).

[28] A. Yoshizawa, S.I. Itoh and K. Itoh, *Plasma and fluid turbulence: theory and modelling* (CRC Press, 2002).